

Electronic Supplementary Material (ESI) for Chemical Communications.

This journal is @The Royal Society of Chemistry 2022

Supporting Information

CO Oxidation over Embedded Pt Nanoparticles on Al₂O₃ with Al Coordination Flexibility

Xiang Wang,^{a, c†} Shuangqin Zeng,^{b†} Guodong Qi,^{*a, c} Qiang Wang,^{a, c} Jun Xu^{*a, c} and
Feng Deng^{a, c}

*Corresponding author

E-mail: qgdong@wipm.ac.cn; xujun@wipm.ac.cn

Contents:

Experimental Section

Catalyst preparation

Catalyst characterization

Evaluation of the catalytic performance

Figure S1. Pore size distribution of cf-Al₂O₃ and γ -Al₂O₃.

Figure S2. SEM images (a) and XRD patterns (b) of cf-Al₂O₃ and γ -Al₂O₃.

Table S1. ICP-OES analysis of Pt content for different samples.

Figure S3. TEM images of Pt loaded cf-Al₂O₃ (left) and γ -Al₂O₃ (right) catalysts with different metal loading amount from 0.2 wt.% to 10 wt.%.

Figure S4. XPS spectra of Pt/cf-Al₂O₃ and Pt/ γ -Al₂O₃ with 1% and 5% Pt loadings.

Figure S5. IR spectra of CO adsorbed on Pt/cf-Al₂O₃ (a) and Pt/ γ -Al₂O₃ (b) with different Pt loading.

Table S2. Pt nanoparticles size for different samples.

Table S3. Comparison of the TOF for CO oxidation on Pt/cf-Al₂O₃ and Pt/ γ -Al₂O₃ catalysts with different Pt loading.

Figure S6. CO oxidation stability on Pt/cf-Al₂O₃ and Pt/ γ -Al₂O₃ with 5% (a) and 10% (b) Pt loading. Reaction conditions: 2.5 vol% CO, 2.5 vol% O₂ and balance He, GHSV: $6 \times 10^4 \text{ h}^{-1}$.

Figure S7. ²⁷Al MAS NMR spectra of cf-Al₂O₃ (a), 1%Pt/cf-Al₂O₃ (b) and 5%Pt/cf-Al₂O₃ (c) with different chemical vapor deposition temperature.

Table S4. Evolution of Al species on cf-Al₂O₃, 1%Pt/cf-Al₂O₃ and 5%Pt/cf-Al₂O₃ heated at elevating temperature.

Experimental Section

Catalyst preparation

The cf-Al₂O₃ support was prepared by calcination of aluminum ammonium carbonate hydroxide (AACH) precursor at 600 °C. The precursor AACH was synthesized by a hydrothermal method, in which 3.22 g Al(NO₃)₃ and 4.64 g CO(NH₂)₂ were dissolved in 30 ml H₂O, then the transparent mixture was transferred into a 50 mL Teflon-lined stainless-steel autoclave and maintained at 100 °C in an oven for 48 h. After cooling down to room temperature, the white cylindrical solid was filtered and washed with appropriate amount of ultrapure water and absolute ethyl alcohol, then the solid was dried at 60 °C overnight^{1, 2}. γ-Al₂O₃ was synthesized by a classical method, in which pseudo boehmite was calcined at 600 °C for 12 h with a ramp rate of 3 °C/min³.

Vacuum decomposition of platinum acetylacetonate was employed to introduce Pt nanoparticles on cf-Al₂O₃ and γ-Al₂O₃ supports. Different amounts of platinum acetylacetonate (1.6mg, 0.2%; 8 mg, 1%; 40mg, 5%; 80mg; 10%) and 400 mg support were mixed and grounded for uniformity. The mixture was transferred to a vacuum line-connected quartz glass tube. After degassing 30 minutes to remove the residual air, the sample was heated in a high-temperature furnace at 3 °C/min until the temperature reached 600 °C and maintained for 10 minutes. The sample turned black quickly as platinum acetylacetonate pyrolyzed. The quartz glass tube was rapidly cooled down with liquid nitrogen to prevent platinum oxidation.

Catalyst characterization

X-ray diffraction (XRD) patterns were recorded on a Panalytical X' Pert PRO X-ray diffractometer (40 kV, 40 mA) using CuKα1 (λ=1.5406 Å) radiation.

Transmission electron microscopy (TEM) images were obtained on a FEI Tecnai G20 instrument at an accelerating voltage of 200 Kv

CO Diffuse Reflectance FTIR spectroscopy (CO-DRIFTS) measurements were performed on a Bruker Tensor 27 instrument. 120 mg Pt/cf-Al₂O₃ or Pt/ γ-Al₂O₃ catalyst with 90% KBr was packed into the in situ FTIR cell in a glovebox under dry

nitrogen atmosphere. The cell was connected to a vacuum apparatus and degased with a pressure below 10^{-3} Pa before adsorption of CO (99.999%, 5 kPa). The DRIFT spectra were recorded by a mercury-cadmium-telluride (MCT) detector with 128 scans at 4 cm^{-1} resolution. KBr was used for collecting the background spectrum.

^{27}Al magic angle spinning solid-state nuclear magnetic resonance (^{27}Al MAS NMR) was recorded on 18.8T using a Bruker Avance III 800 spectrometer and a 3.2 mm double resonance probe. The resonance frequency was 208.54 MHz for ^{27}Al . A pulse width of $0.3\ \mu\text{s}$ corresponding to a $\pi/12$ flip-angle and a recycle delay of 2 s were used to record the single-pulse ^{27}Al MAS NMR spectrum at a spinning speed of 20 kHz. The ^{27}Al chemical shifts were referenced to 1M $\text{Al}(\text{NO}_3)_3$ aqueous solution (0 ppm).

BET analysis was carried out on a Micromeritics ASAP-2010 Analyzer to measure the surface area.

X-ray photoelectron spectroscopy (XPS) characterization was performed on a Thermo VG Scientific ESCA Multilab-2000 spectrometer (Thermo Electron Corporation). Monochromatized Al $K\alpha$ (1486.7 eV) was used as the X-ray source.

CO oxidation reaction

For CO oxidation light-on curves measurements, 100 mg catalyst was calcined by air at $400\text{ }^\circ\text{C}$ for 2h. The catalyst was then reduced in-situ with 5 vol % H_2 and N_2 at $400\text{ }^\circ\text{C}$ for 2 h in a quartz-tube fixed bed reactor. After being cooled to room temperature, the feed gas containing 2.5 vol % CO, 2.5 vol % O_2 and balance He was allowed to pass through the reactor at a flow rate of $80\text{ ml}\cdot\text{min}^{-1}$ corresponding to a gas hourly space velocity (GHSV) of $4.8\cdot 10^4\text{ h}^{-1}$. The catalyst was heated to the desired temperatures at a rate of 2°C min^{-1} and then kept for 30 min until the catalytic reaction reached a steady state. Carbon monoxide oxidation tests under different GHSV were performed at the T100 temperature by using 20 mg catalyst, and the flow rate of feed gas varied from 80 ml to 10 ml corresponding to GHSV of $3\cdot 10^4\text{ h}^{-1}$, $6\cdot 10^4\text{ h}^{-1}$, $1.2\cdot 10^5\text{ h}^{-1}$ and $2.4\cdot 10^5\text{ h}^{-1}$, respectively after 30 min reaction time to reach a steady state.

Long-term CO oxidation tests were performed at the T_{100} temperature using 20 mg cf- Al_2O_3 and $\gamma\text{-Al}_2\text{O}_3$ with 5% and 10% Pt loading, and the GHSV was $2.4 \times 10^5 \text{ h}^{-1}$ (keeping CO conversion below 20%).

The composition of effluent gas was analyzed by a gas spectrometer (GC 2014, Shimadzu, Japan) equipped with a packed column (TDX-1) and a methane converter in front of a flame ionization detector (FID). The methane converter is a micro high-temperature furnace (375 °C) with Ni-based catalyst that can fully convert CO and CO_2 into CH_4 for FID detection. The CO conversion was calculated from the change in CO_2 concentration of the inlet and outlet gases. The TOF calculation is based on the previous literature report and assumes 100% Pt dispersion for all catalyst samples⁴.

The TOF for CO oxidation was calculated by the following method:

$$TOF = \frac{F * \alpha}{V_m * N * w}$$

F= flow rate of CO (1/s)

α = conversion of CO

V_m = molar volume (24.4 L/mol)

N= moles of surface Pt atoms per gram catalyst (mol/g)

w= weight of the catalyst in the reactor (g)

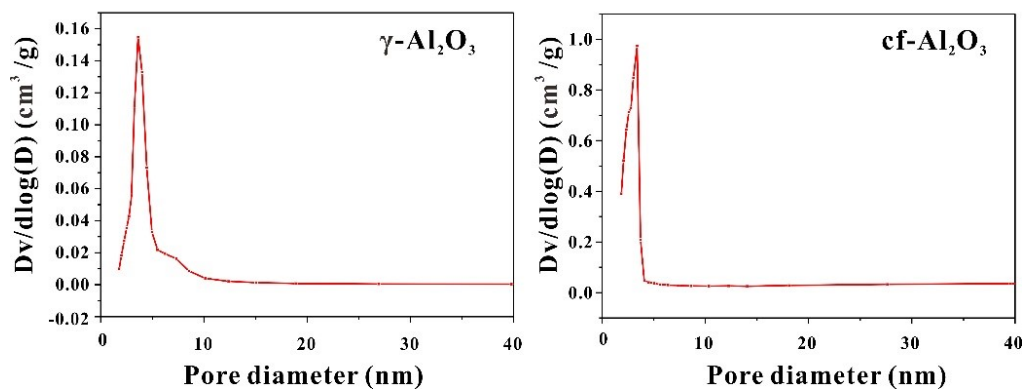


Figure S1. Pore size distribution of cf- Al_2O_3 and $\gamma\text{-Al}_2\text{O}_3$.

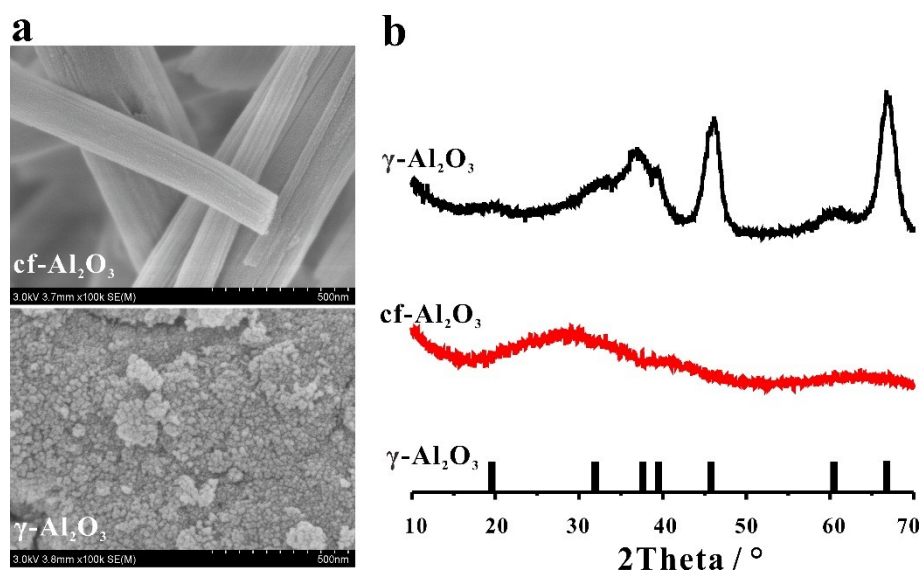


Figure S2. SEM images (a) and XRD patterns (b) of $\text{cf-Al}_2\text{O}_3$ and $\gamma\text{-Al}_2\text{O}_3$.

Table S1. ICP-OES analysis of Pt content for different samples.

Samples	Actual Pt loading (wt.%)	Target Pt loading (wt.%)
0.2Pt/ γ -Al ₂ O ₃	0.20	0.2
1Pt/ γ -Al ₂ O ₃	0.82	1
5Pt/ γ -Al ₂ O ₃	4.1	5
10Pt/ γ -Al ₂ O ₃	7.26	10
0.2Pt/cf-Al ₂ O ₃	0.17	0.2
1Pt/cf-Al ₂ O ₃	0.75	1
5Pt/cf-Al ₂ O ₃	3.59	5
10Pt/cf-Al ₂ O ₃	7.55	10

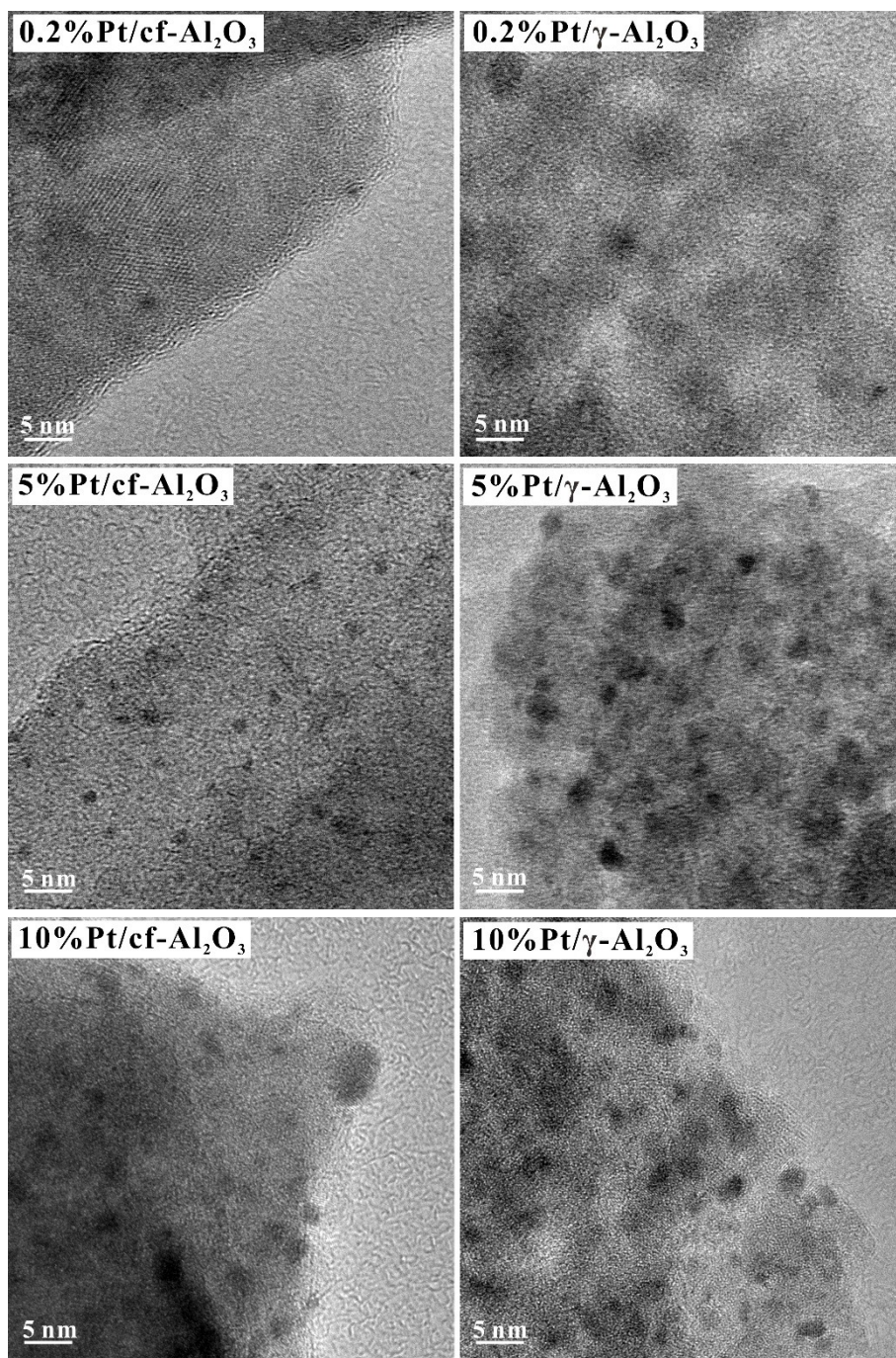


Figure S3. TEM images of Pt loaded cf-Al₂O₃ (left) and γ-Al₂O₃ (right) catalysts with different metal loading amount from 0.2 wt.% to 10 wt.%.

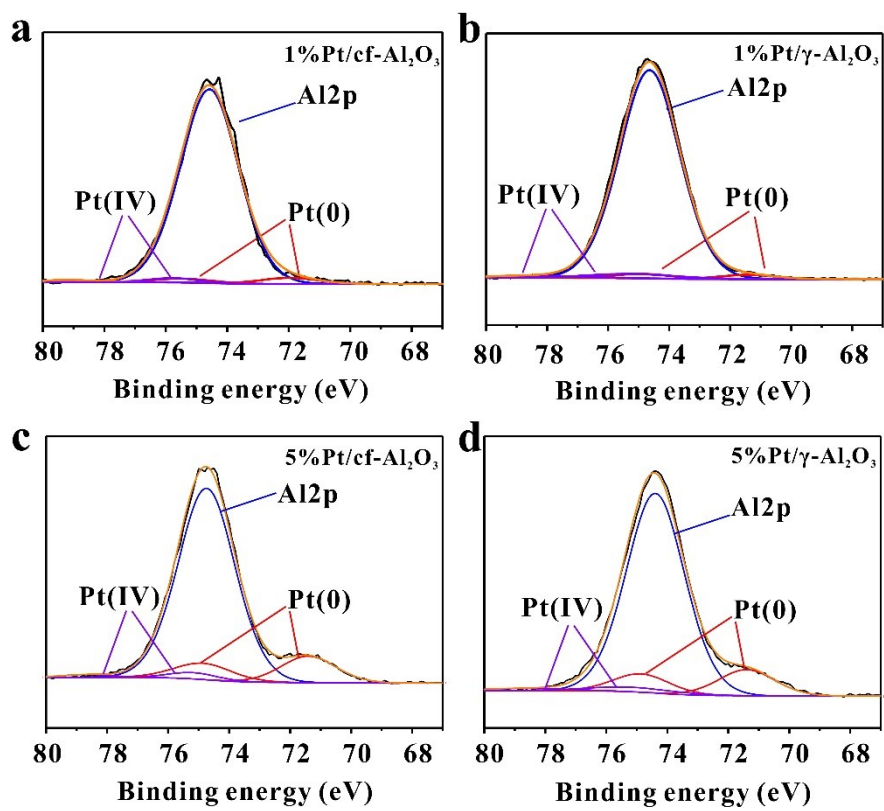


Figure S4. XPS spectra of Pt/cf-Al₂O₃ and Pt/ γ -Al₂O₃ with 1% and 5% Pt loadings.

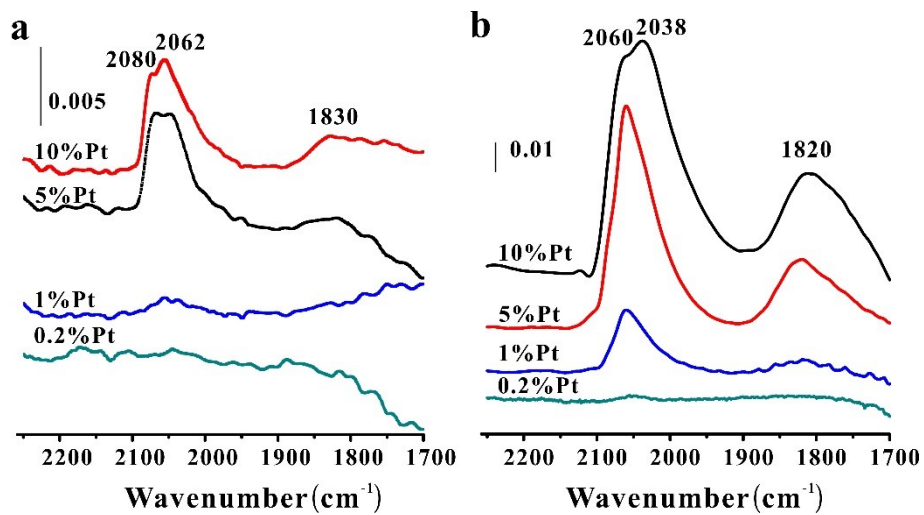


Figure S5. IR spectra of CO adsorbed on Pt/cf-Al₂O₃ (a) and Pt/γ-Al₂O₃ (b) with different Pt loading.

Table S2. Pt nanoparticles size for different samples.

Samples	Pt nanoparticles size (nm)
0.2%Pt/ γ -Al ₂ O ₃	0.93 ± 0.29
1%Pt/ γ -Al ₂ O ₃	1.21 ± 0.22
5%Pt/ γ -Al ₂ O ₃	1.25 ± 0.25
10%Pt/ γ -Al ₂ O ₃	1.28 ± 0.27
0.2%Pt/cf-Al ₂ O ₃	0.68 ± 0.02
1%Pt/cf-Al ₂ O ₃	0.92 ± 0.11
5%Pt/cf-Al ₂ O ₃	1.07 ± 0.19
10%Pt/cf-Al ₂ O ₃	1.70 ± 0.48

Table S3. Comparison of the TOF for CO oxidation on Pt/cf-Al₂O₃ and Pt/ γ -Al₂O₃ catalysts with different Pt loading.

Supports	Pt loading (wt.%)	CO/O ₂	T(°C)	Conversion (%)	TOF (s ⁻¹)	Notes
cf-Al ₂ O ₃	0.2		260	7.14	0.560	
	1		220	6.50	0.115	
	5	2.5%CO	170	4.12	0.015	
	10	2.5%O ₂	150	4.48	0.008	This work
γ -Al ₂ O ₃	0.2	95%He	240	5.68	0.378	
	1		200	5.58	0.093	
	5		160	3.22	0.010	
	10		150	3.90	0.007	
m-Al ₂ O ₃ -H ₂	0.2	2.5%CO 2.5%O ₂ 95%Ar	250	13.2	0.175	Ref. ⁵
θ -Al ₂ O ₃	0.18	3.7%CO 3.7%O ₂ 93.6%He	251	~10	0.187	Ref. ⁶
Al ₂ O ₃	0.4	25%CO 25%O ₂ 50%balance	150	~10	0.005	Ref. ⁴

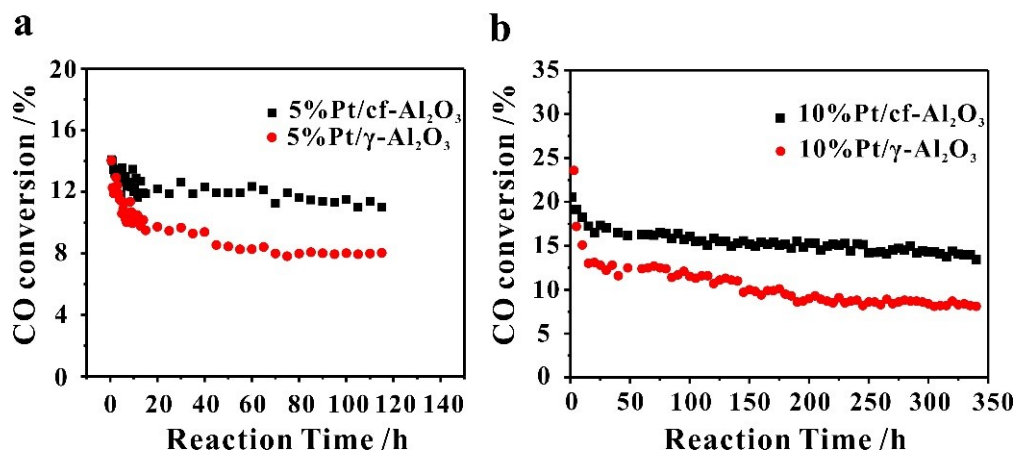


Figure S6. CO oxidation stability on Pt/cf-Al₂O₃ and Pt/γ-Al₂O₃ with 5% (a) and 10% (b) Pt loading. Reaction conditions: 2.5 vol% CO, 2.5 vol% O₂ and balance He, GHSV: 6*10⁴ h⁻¹.

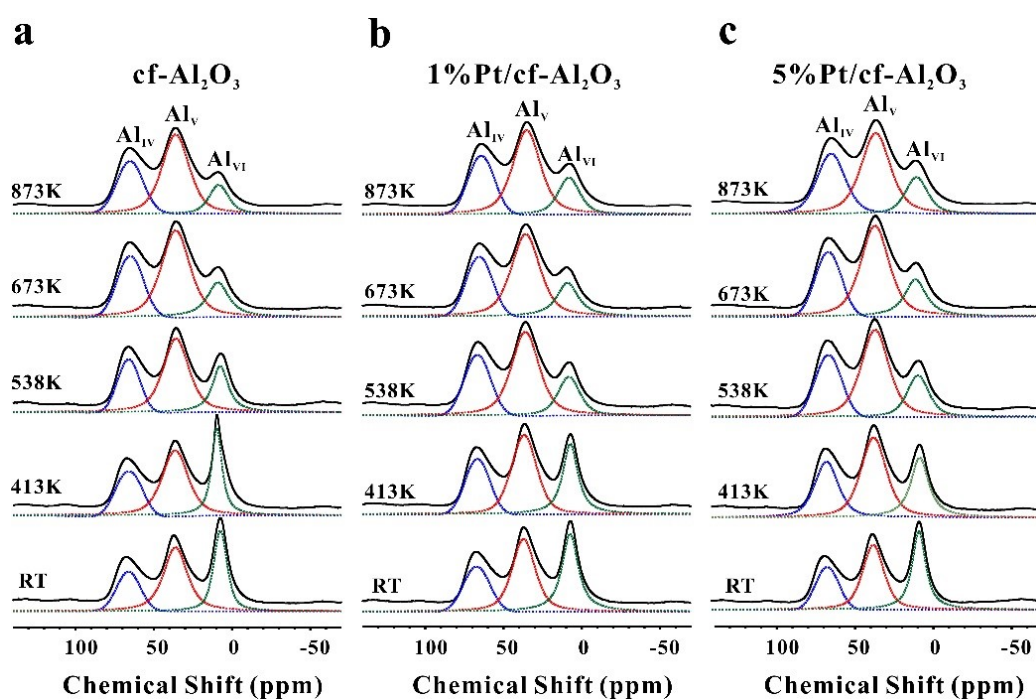


Figure S7. ^{27}Al MAS NMR spectra of $\text{cf-Al}_2\text{O}_3$ (a), $1\% \text{Pt/cf-Al}_2\text{O}_3$ (b) and $5\% \text{Pt/cf-Al}_2\text{O}_3$ (c) with different chemical vapor deposition temperature.

Table S4. Evolution of Al species on cf-Al₂O₃, 1%Pt/cf-Al₂O₃ and 5%Pt/cf-Al₂O₃ heated at elevating temperature.

Support	Temperature	Al _{IV} (%)	Al _V (%)	Al _{VI} (%)
cf-Al ₂ O ₃	RT	20.9	44.4	34.7
1%Pt/cf-Al ₂ O ₃		22.7	41.3	36.0
5%Pt/cf-Al ₂ O ₃		22.9	40.8	36.3
cf-Al ₂ O ₃	413K	22.9	47.6	29.5
1%Pt/cf-Al ₂ O ₃		25.6	44.8	29.6
5%Pt/cf-Al ₂ O ₃		28.4	44.4	27.2
cf-Al ₂ O ₃	538K	24.6	52.4	23.0
1%Pt/cf-Al ₂ O ₃		28.4	52.6	19.0
5%Pt/cf-Al ₂ O ₃		27.9	52.6	19.4
cf-Al ₂ O ₃	673K	27.4	53.8	18.8
1%Pt/cf-Al ₂ O ₃		28.2	53.2	18.6
5%Pt/cf-Al ₂ O ₃		27.8	53.5	18.7
cf-Al ₂ O ₃	873K	26.5	54.0	19.5
1%Pt/cf-Al ₂ O ₃		26.5	54.0	19.5
5%Pt/cf-Al ₂ O ₃		26.5	54.0	19.5

References

1. L. Shi, G. M. Deng, W. C. Li, S. Miao, Q. N. Wang, W. P. Zhang and A. H. Lu, *Angew. Chem. Int. Ed.*, 2015, **54**, 13994-13998.
2. Z. Zhao, D. Xiao, K. Chen, R. Wang, L. Liang, Z. Liu, I. Hung, Z. Gan and G. Hou, *ACS Cent. Sci.*, 2022, **8**, 795-803.
3. S. J. Wilson, *Mineral. Mag.*, 1979, **43**, 301-306.
4. Y. J. Mergler, A. vanAalst, J. vanDelft and B. E. Nieuwenhuys, *Appl. Catal., B*, 1996, **10**, 245-261.
5. Z. L. Zhang, Y. H. Zhu, H. Asakura, B. Zhang, J. G. Zhang, M. X. Zhou, Y. Han, T. Tanaka, A. Q. Wang, T. Zhang and N. Yan, *Nat. Commun.*, 2017, **8**.
6. M. Moses-DeBusk, M. Yoon, L. F. Allard, D. R. Mullins, Z. L. Wu, X. F. Yang, G. Veith, G. M. Stocks and C. K. Narula, *J. Am. Chem. Soc.*, 2013, **135**, 12634-12645.